Cent. Eur. J. Geosci. • 4(2) • 2012 • 246-260
DOI: 10.2478/s13533-011-0055-x

VERSITA

Central European Journal of **Geosciences**

Easily altered minerals and reequilibrated fluid inclusions provide extensive records of fluid and thermal history: gypsum pseudomorphs of the Tera Group, Tithonian-Berriasian, Cameros Basin

Research Article

Laura González-Acebrón[1], Robert H. Goldstein[2], Ramon Mas[1], Jose Arribas[3]

1 *Dpto. Estratigrafía, Facultad de Ciencias Geológicas, Universidad Complutense de Madrid (UMC) – Instituto de Geociencias (IGEO, CSIC-UCM), Madrid, Spain*

2 *Department of Geology, University of Kansas, Lawrence, Kansas, USA.*

3 *Dpto. Petrología y Geoquímica. Facultad de Ciencias Geológicas, Universidad Complutense de Madrid (UCM) – Instituto de Geociencias (IGEO, CSIC-UCM), Madrid, Spain*

Received 30 October 2011; accepted 30 January 2012

Abstract: This study reports a complex fluid and thermal history using petrography, electron microprobe, isotopic analysis and fluid inclusions in replacement minerals within gypsum pseudomorphs in Tithonian-Berriasian lacustrine deposits in Northern Spain. Limestones and dolostones, formed in the alkaline lakes, contain lenticularly shaped gypsum pseudomorphs, considered to form in an evaporative lake. The gypsum was replaced by quartz and non-ferroan calcite (Ca-2), which partially replaces the quartz. Quartz contains solid inclusions of a preexisting non-ferroan calcite (Ca-1), anhydrite and celestine.

High homogenization temperatures (T_h) values and inconsistent thermometric behaviour within secondary fluid inclusion assemblages in quartz (147-351°C) and calcite (108-352°C) indicate high temperatures after precipitation and entrapment of lower temperature FIAs. Th are in the same range as other reequilibrated fluid inclusions from quartz veins in the same area that are related to Cretaceous hydrothermalism.

Gypsum was replaced by anhydrite, likely during early burial. Later, anhydrite was partially replaced by Ca-1 associated with intermediate burial temperatures. Afterward, both anhydrite and Ca-1 were partially replaced by quartz and this by Ca-2. All were affected during higher temperature hydrothermalism and a CO_2-H_2O fluid. Progressive heating and hydrothermal pulses, involving a CO_2-H_2O fluid, produce the reequilibration of the FIAs, which was followed by uplift and cooling.

Keywords: Fluid inclusions • gypsum pseudomorphs • Cameros Basin • thermal reequilibration

1. Introduction

This study provides an example of the use of easily altered geologic materials (lenticular gypsum, calcite, fluid inclusions in calcite and quartz) to ascertain a complex diagenetic, fluid, and thermal history as well as events of hydrothermal metamorphism. In such easily altered materials, one might typically determine that no record is preserved, but this study shows that easily replaced soluble minerals, such as gypsum, provide the medium for

partial replacement to preserve complexities of the fluid and thermal history, despite, or perhaps as result of, significant replacement and thermal alteration.

Although macroscopic gypsum crystals occur in a variety of habits, one of the most widespread in distribution and environmental significance is lenticular gypsum. Lenticular gypsum crystals occur in many parts of the world in present-day sediments and in ancient rocks [1] and is usually considered to form early and displacively in association with evaporative conditions.

Replacement of gypsum by calcite is known in various diagenetic environments. It can happen at low temperature soon after gypsum precipitation as well as during uplift; it can also happen in the deep burial environment, commonly associated with hydrocarbon migration and thermochemical sulphate reduction [2]. The absence of compactional textures and strained crystal forms in gypsum pseudomorphs is commonly used to interpret them as early diagenetic replacements [3]. In our case we observe non-deformed well-preserved pseudomorphs that have had a highly complex replacement history over an extended period of time.

Petrography, fluid inclusion, electron microprobe, and stable isotope studies in gypsum pseudomorphs and their host-rocks from a Tithonian-Berriasian lacustrine sedimentary sequence Northern Spain provides evidence for multiple episodes of lenticular gypsum replacement in different diagenetic environments, overprinted by hydrothermal metamorphism. This work pinpoints the importance of combining petrography of replacement phases and solid inclusions with electron microprobe, cold-cathodoluminescence, isotopic geochemistry and fluid inclusion study in easily replaced minerals or thermally altered fluid inclusions. The partial alteration of the minerals and the fluid inclusions, including those affected by natural thermal reequilibration, preserve a record of fluid and thermal history that might not otherwise have been preserved in unaltered materials. As most workers shy away from such materials as too easily altered, this study demonstrates a contrasting finding that partial preservation of easily altered materials may be the key in better refining the fluid and thermal history of a basin.

2. Geological setting

2.1. Basin formation

The Cameros Basin in the northern Iberian Range (Fig. 1) is part of the Mesozoic Iberian Rift System [4–7]. Intraplate rifting was a consequence of a generalized extensional regime, which separated Iberia from Europe.

The subsidence and sedimentation rates in Cameros Basin were very high, with vertical thicknesses up to 6 km, and up to 9 km of stratigraphic record in the direction of the northward migration of depositional sequences recorded from the Tithonian to the early Albian. The basin has been interpreted as a hanging wall synclinal basin (extensional-ramp basin). It formed over a roughly south-dipping ramp between two nearly horizontal sections (flats) in a deep extensional fault (detachment) inside the 7 to 11 km-deep Variscan Basement. The direction of displacement for the hanging wall was S-SW, parallel to the direction of the basin extension [4, 5, 7–9].

Alternatively, Guiraud and Seguret [10], Casas-Sainz and Gil-Imaz [11], Mata et al. [12], Villalaín et al. [13] and Casas-Sainz et al. [14] interpreted the Cameros Basin as a synclinal basin, with vertical superposition of Lower Cretaceous sedimentary units rather than laterally juxtaposed bodies onlapping the prerift sequence. These authors consider a thrust fault to the north as a result of tectonic inversion of a normal fault generated at the beginning of the Cretaceous, which reached the Keuper facies at depth. It has been suggested that this hypothesis has a mechanical flaw that makes it unlikely [4, 5, 7, 9]. The hypothesis would require a slab of Jurassic rocks, only 500-800 m thick but more than 30 km wide and 100 km long, to be pulled from the South without suffering any break in continuity and without forming a fault over the ramp near the northern basin margin. This would have had to occur under subaerial conditions because of the continental nature of the rocks that filled the basin. Their model would require, an even more difficult to produce, later reverse displacement of tens of kms to the North, still somehow maintaining the continuity of the thin marine Jurassic slab after the Cenozoic contraction.

2.2. Stratigraphy

The basin record essentially consists of continental sedimentary rocks corresponding to alluvial and lacustrine systems, with rare marine incursions [4, 15]. Figure 1 shows the location of the studied stratigraphic sections. The sedimentary infill of the Cameros Basin has been divided into eight depositional sequences [7, 9]. The Tera Group represents the first stage of rifting sedimentation and is formed by two depositional sequences (DS 1 and DS 2), which are Tithonian-Berriasian in age [4, 16, 17]. DS 1 is represented by siliciclastic alluvial fan facies and lacustrine-palustrine carbonate facies. The thickness of DS 1 is highly variable, with maximum thickness of 255 m [18]. DS 2 is up to 1500 m-thick in the depocentre, and consists of siliciclastic fluvial facies, which grade upwards and laterally to carbonate lacustrine facies. At

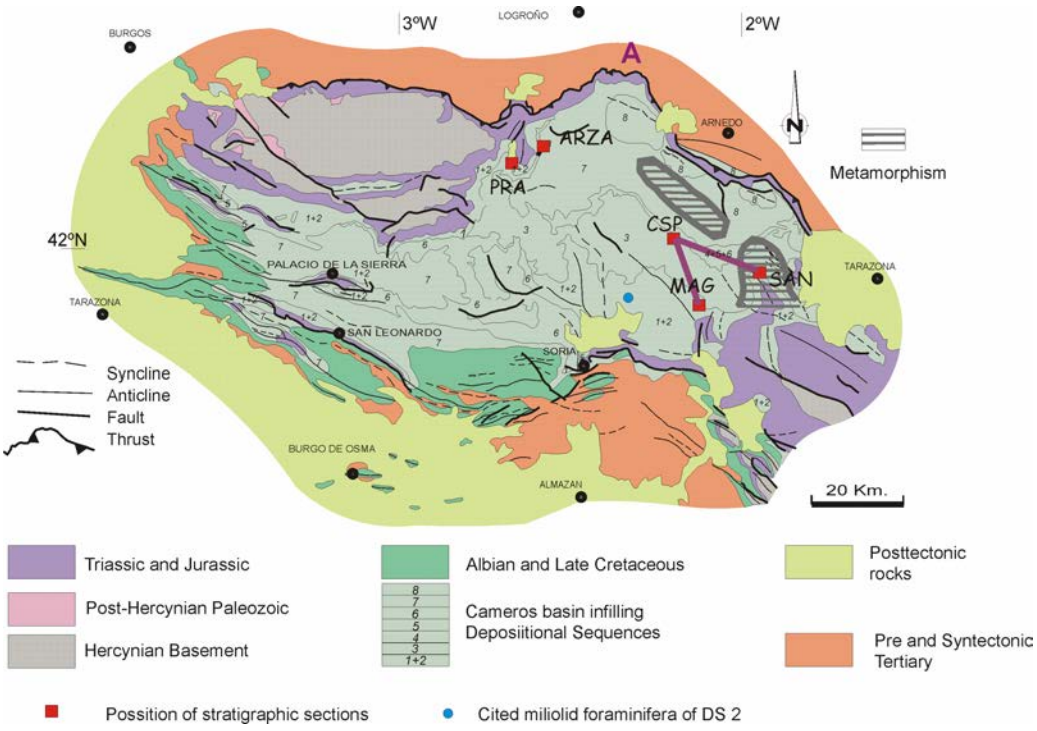

Figure 1. Geologic map of the Cameros Basin showing the areas affected by metamorphism. The positions of the stratigraphic sections of the Tera Group are also marked: ARZA: Almarza. PRA: Pradillo. CSP: El Collado de San Pedro. MAG: Magaña. SAN: San Felices. Cited miliolid foraminifera by Gómez-Fernández and Meléndez [15]. Position of a stratigraphic cross section (Fig. 2) marked with purple line.

the top of DS 2, Gómez-Fernández and Meléndez [15] proposed minor marine influence towards the SW of the studied area (see blue dot in Fig. 1) based on the presence of foraminifera.

This study is focused on the lacustrine facies of DS 2. The analysis of these lacustrine facies reveals the following evolution: (1) shallow carbonate ramps in lakes; to (2) shallow alkaline ephemeral lakes and then (3) carbonate lakes rich in organic matter [19]. This facies evolution indicates that these lakes evolved from open to more closed hydrologic conditions, also experiencing variations in nutrients and climate. The cause in part may be a local tectonic one, with progressive rift development and faulting leading to progressive isolation. All three types of lacustrine facies are found only in the southern part of the study area (Fig. 2, MAG, CSP, SAN), whereas in the northern part, lacustrine facies only appear in ARZA section and consist only of shallow carbonate ramp lacustrine facies.

2.3. Metamorphic processes

During the Late Albian to Coniacian, hydrothermal alteration affected the deposits of the Eastern sector of the Cameros Basin, in SAN area (Fig. 1) [19–26]. The main features of this thermal alteration are: (1) metamorphic grade is controlled by changes in rock composition and permeability rather than by burial depth [20, 21, 27, 28]; (2) thermal inversions across sections in the depocentre [24, 25, 28]; (3) post-rift age of alteration (107±5 to 85±6 My dated by K-Ar on authigenic illites [19] or 99±2 My by U-Pb SHRIMP on monazites [29]) after the maximum burial stage, reached during the Early Albian; and (4) metamorphic conditions from very low-grade (anchizone) to low-grade (epizone), with temperatures of 350-370°C at the metamorphic peak and maximum pressure of 1 Kbar [19, 20]. Lines of evidence 1 and 2 point to a hydrothermal process rather than the regional metamorphic model suggested by Guiraud and Seguret [10], Casas-Sainz and Gil-Imaz [11] and Mata et al. [12].

The Tera Group was buried to 5900 m from the Tithonian to Lower Paleogene at the more depocentral section (SAN, Fig. 1). Burial depth is based on partial restored cross-sections from Guimerá et al. [5] and Mas et al. [9].

3. Sampling and analytical methods

A total of 45 samples were collected systematically from five representative stratigraphic sections of the DS2 la-

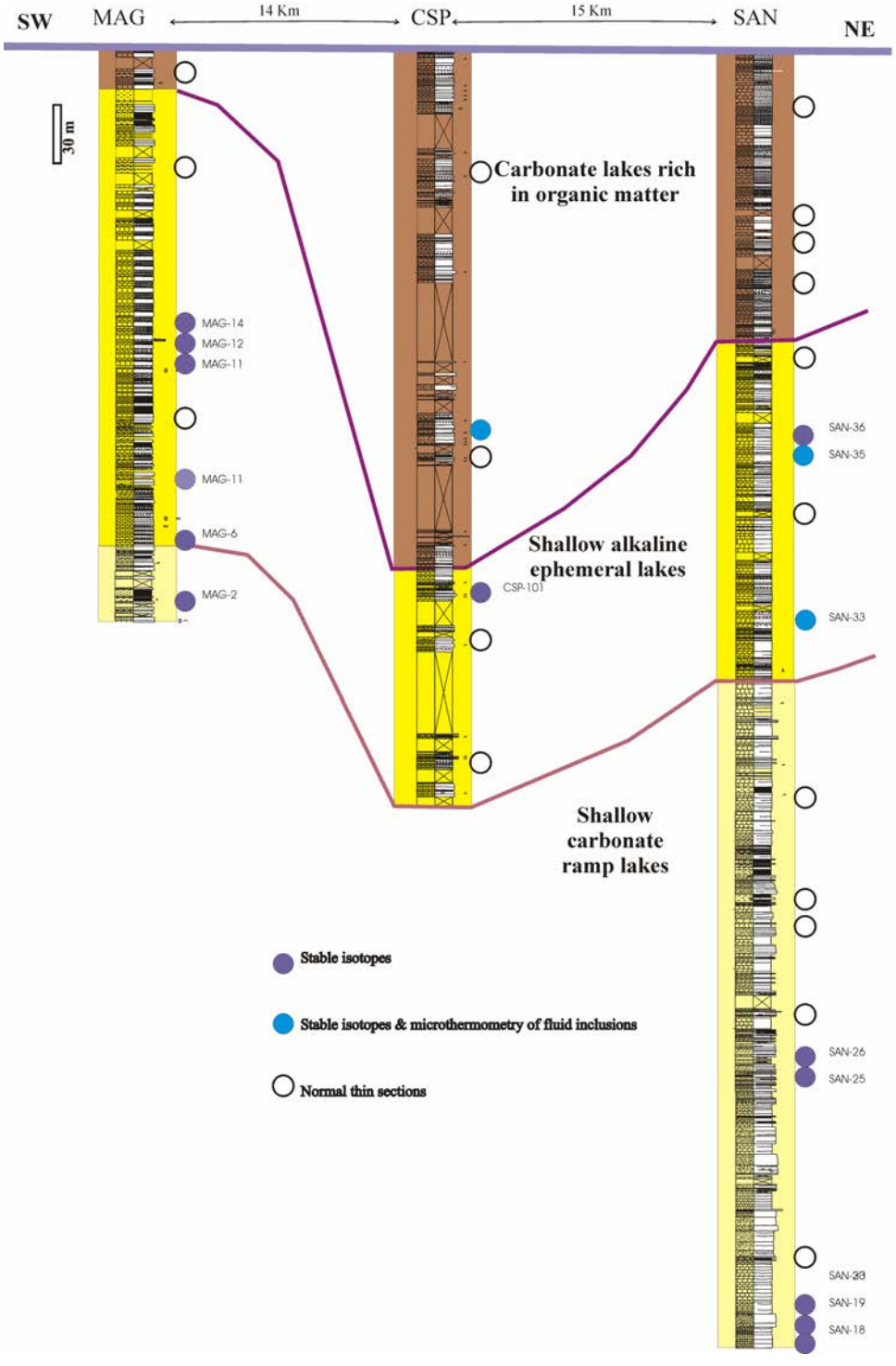

Figure 2. Stratigraphic cross section of the lacustrine record in the southern part of the study area of the Cameros Basin. The location is marked in Fig. 1. For names of the stratigraphic section see caption of Fig. 1. Positions of samples are shown. Thin sections have been represented with a different pattern than those samples in which petrography has been combined with stable isotope study and microthermometry by using both thin and thick sections.

custrine facies of the Tera Group (Figs. 1, 2), trying to represent the vertical variation. For each sample, a polished epoxy-mounted 30 μm thin section was prepared. In addition, ten doubly polished selected thick sections were prepared for fluid inclusion study without any heating and glued to frosted glass with cyanoacrilate. After optical petrographic analysis of these sections, selected areas of 4 of these sections were cut and removed from the glass using acetone. The microthermometric study was performed on these portions of samples in a Linkam THMSG-600 heating and freezing stage. The stage was calibrated with synthetic fluid inclusions, including triple point of CO_2, melting point of H_2O, and critical point of H_2O. The accuracy for low-temperature measurements is better than ±0.1°C and for high temperature measurements are better than ±1.0°C.

Abbreviation for homogenization temperature is T_h, for final melting temperature of ice is T_m(ice), for nucleation temperature is T_n, for clathrate nucleation temperature is T_n(cl) and for final melting temperature of clathrate is T_m(cl). The T_h have been interpreted as minimum entrapment temperatures. In this case, pressure corrections were not applied because a pressure determination would involve too many error-prone assumptions without independent pressure estimation methods. Representing T_h as minimum entrapment temperatures is a typical procedure in interpreting T_h data [29, 30]. To interpret salinity from T_m(ice), a NaCl-H_2O model was used on the basis of the observed first melting temperatures from fluid inclusions [32], and the NaCl-H_2O-CO_2 model system when clathrates are observed. The calculations employed the ICE software [33].

Sixteen epoxy-mounted 150 μm-thick sections were prepared on carbonate bearing pseudomorphs. CL examination was carried out using a Technosyn® cold cathodoluminescence unit operating at 14-17 KV with 350-450 μA beam current. These sections were etched and stained using Alizarin Red S and potassium ferricyanide for carbonate identification [34] after cathodoluminescence (CL) study. Carbonate samples were taken using a microdrill and analyzed for $\delta^{13}C$ and $\delta^{18}O$. Carbonate minerals from both gypsum pseudomorphs and their host rock were taken to obtain coupled values in the same sample (if there was enough material for each one). This helped in distinguishing between depositional, early, and late diagenetic signatures. Where abundant enough, samples were also taken for $^{87}Sr/^{86}Sr$ analysis (six samples). Analyses of $\delta^{13}C$ and $\delta^{18}O$ were performed at the Keck Paleoenvironmental and Environmental Stable Isotope Laboratory (KPESIL) at the University of Kansas. Strontium isotopes were performed in the laboratory of Isotopic Geochronology and Geochemistry of the Complutense University of Madrid.

For stable isotope analysis, all sample powders were roasted in vacuum for one hour at 200°C to remove volatile organic contaminants, and afterward reacted at 73°C in an automated carbonate reaction system (Kiel-III) coupled directly to the inlet of a Finnigan MAT 253 gas ratio mass spectrometer. Isotopic ratios were collected for ^{17}O contribution and are reported in per mil notation relative to the VPDB standard. Values were calibrated using NBS-19 as the primary standard. The precision of the analysis is 0.1‰ for both Oxygen and Carbon.

For $^{87}Sr/^{86}Sr$, dolomite or calcite powder was dissolved in 2 mL of a solution of 2.5N HCl, later evaporated to dryness at 80-100°C. Samples were re-dissolved in 2.5N HCl solution and Sr was pre-concentrated by standard methods of column chromatography. Following this, the Sr-concentrated samples were dissolved in 2 mL of phosphoric acid and Sr isotopic ratios were then determined with a VG SECTOR 54 five-collector mass spectrometer. Isotopic ratios were corrected for possible interferences from ^{87}Rb and normalized to the value of $^{87}Sr/^{86}Sr = 0.1194$, to correct the isotopic fractionation effect. Analytical precision was monitored by analysis of NBS-987 standard and measurement precision was maintained at better than $\pm 5{\cdot}10^{-5}$.

A Jeol JXA-8900 M electron microprobe was used to characterize major and minor element composition of the samples. Operating conditions were 15 kV, 20 nA and 5 μm beam diameter. Measured oxide standards were CaO, Na_2O, SrO, MgO, FeO and MnO, and mean detection limits were 130, 110, 140, 130, 310 and 330 ppm for each element respectively.

4. Results

4.1. Petrography of the lacustrine facies and the gypsum pseudomorphs

The lowermost occurrences of carbonate deposits are associated with meandering fluvial systems of DS 2 (ARZA, PRA: Figs. 1, 2). Laterally and towards the top of the stratigraphy (CSP, MAG, SAN: Figs. 1, 2) carbonate facies are related to shallow carbonate ramp lacustrine facies [18]. Strata are lime mudstone and dolostone with ostracodes and characea, with very sparse gastropods and interlayered with channelized fine-grained sandstones.

Towards the eastern part of the study area (CSP, MAG, SAN: Fig. 1, 2) and at the top of the stratigraphic succession, there is evidence of shallow alkaline ephemeral lakes [18]. This facies association contains the gyp-

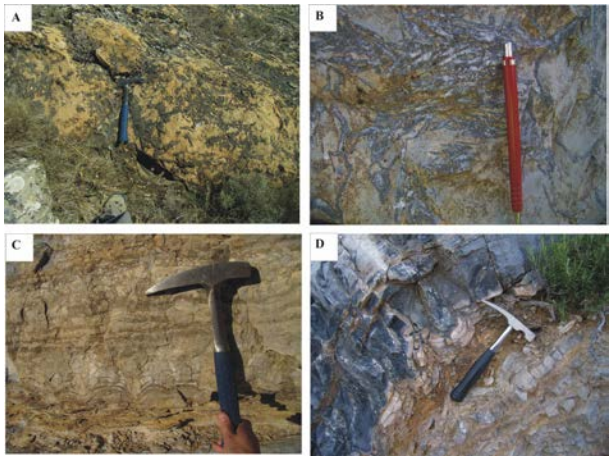

Figure 3. Field photographs of lacustrine deposits of DS 2. **A.** Abundant lenticular gypsum pseudomorphs in micritic limestone. **B.** Swallow-tail lenticular gypsum pseudomorphs. **C.** Domal stromatolites and autoclastic breccias in lacustrine sequences. **D.** Tepee at the top of the sequence.

sum pseudomorph-bearing layers (Fig. 3**A, B**). These layers are made up by coarsening upward limestone and/or dolostone carbonate sequences with common stromatolites (Fig. 3**C**), autoclastic breccias (Fig. 3**C**) and tepee structures (Fig. 3**D**). Limestones and dolostones formed in these alkaline lakes have a characteristic fetid smell when breaking and contain abundant lenticularly shaped gypsum pseudomorphs.

Gypsum pseudomorph size ranges among different layers from 1 mm to 20 cm long. The concentration of the pseudomorphs in each level is also highly variable. They are irregularly distributed and some have swallow-tail twin morphologies (Fig. 3**A, B**). Gypsum pseudomorphs are for the most part replaced by quartz and non-ferroan calcite (Ca-2, Fig. 4**A, B**). The quartz contains solid inclusions of non-ferroan calcite (Ca-1), anhydrite, and less commonly celestine (Figs. 5**A, B, C**). Solid inclusions are typically oriented in same direction, 40-100 μm-size, rectangular in shape (Fig. 5**A**). Ca-2 calcite also contains solid inclusions of anhydrite, and in a few examples, celestine (Fig. 5**C**).

Small framboidal pyrite crystals (10-100 μm) are commonly observed in the limestone host rock and in the inner boundaries of the pseudomorphs (Fig. 5**D**). The solid inclusions in quartz and Ca-2 calcite are probably relicts of earlier diagenetic processes. Quartz is corroded by Ca-2 calcite supporting that Ca-2 calcite postdates quartz (Fig. 4**B**). Ca-2 calcite is either very clean and non-luminescent under CL, with composition of ($Sr_{0.103}$ $Mg_{0.617}$ $Na_{0.068}$ $Fe_{0.128}$ $Mn_{0.192}$ $Ca_{98.893}$) $(CO_3)_{100}$ and Mg/Ca ratio is 0.006 (n=9) or cloudy with dull orange zoned (in places) CL, with composition of ($Sr_{0.124}$ $Mg_{1.046}$ $Na_{0.019}$ $Fe_{0.321}$ $Mn_{0.251}$ $Ca_{98.238}$) $(CO_3)_{100}$ and Mg/Ca ratio is 0.011 (n=23).

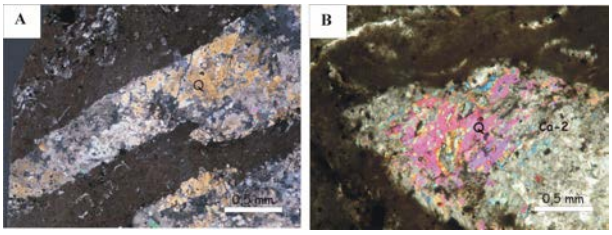

Figure 4. Photomicrographs of gypsum pseudomorphs. Crossed nichols **A.** Gypsum pseudomorph mainly replaced by quartz in a limestone micritic matrix with ostracode fragments. **B.** Non ferroan calcite (Ca-2) and quartz (Q) in gypsum pseudomorph. Notice the corrosion of the quartz by Ca-2.

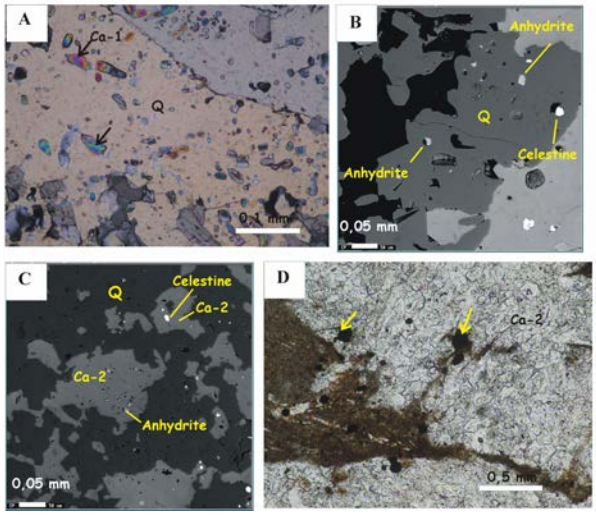

Figure 5. Photomicrographs of gypsum pseudomorphs. **A.** Detail of the solid inclusions of non ferroan calcite (Ca-1, arrows) in quartz (Q). Crossed nichols. **B.** Anhydrite and celestine inclusions in quartz. BSE image. **C.** Anhydrite and celestine inclusions in Ca-2. Notice the corrosion of quartz by Ca-2. BSE image. **D.** Pyrite (arrows) in the micritic limestone host rock and on the inner boundaries of a Ca-2-replaced pseudomorph.

4.2. Stable isotope geochemistry

The microfacies of the above described carbonate strata have been studied in all sections for the stable isotope study. Depositional matrix is either calcitic or dolomitic with micritic texture, showing in some cases microsparitic and pseudosparitic recrystallization fabrics. The most fine-grained micritic matrix was sampled to be most representative of original depositional material for isotopic analysis.

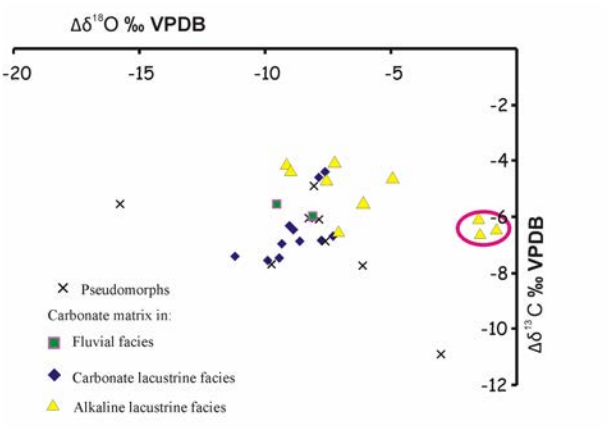

Figure 6. Stable isotope data in relation to the different sedimentary environments.

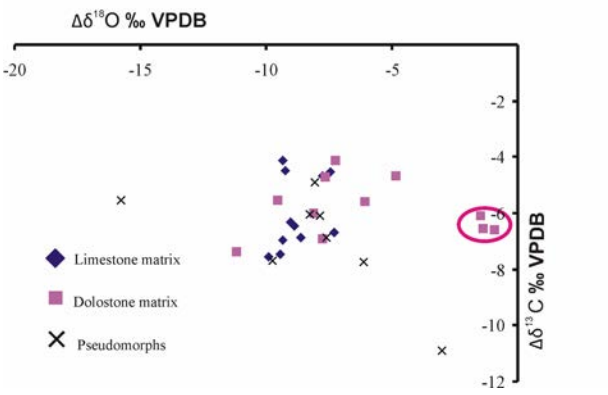

Figure 7. Stable isotope data of limestone and dolostone micritic matrix and Ca-2 in gypsum pseudomorphs. Notice the enrichment in $\delta^{18}O$ of three dolomite matrix samples compared to other matrix samples.

In the lowermost occurrences of carbonate deposits (ARZA, PRA: Figs. 1, 2) only dolomicritic matrix was abundant enough for sampling, and has isotopic values of $\delta^{13}C$= -6.01/-5.53‰ VPDB and $\delta^{18}O$ = -9.54/-8.09‰ VPDB (n=2) (Table 1, Figs. 6, 7).

Towards the top of the stratigraphy (CSP, MAG, SAN: Figs. 1, 2), the limestone has isotopic values of $\delta^{13}C$ = -9.43/-7.44‰ VPDB and $\delta^{18}O$ =-7.56/-4.67‰ VPDB (n=9, ARZA, MAG, SAN) (Table 1, Figs. 6, 7). At the top of the stratigraphic succession (CSP, MAG, SAN: Fig. 1, 2), isotopic values in limestones are $\delta^{13}C$ = -6.67/-4.14‰ VPDB and $\delta^{18}O$ = -9.36/-4.87‰ VPDB (n=7, MAG, SAN) (Table 1, Figs. 6, 7), and in dolostones are $\delta^{13}C$ =-6.59/-6.11‰ VPDB and $\delta^{18}O$ = -1.48/-0.94‰ VPDB (n=3, MAG) (Table 1, Figs. 6, 7).

In the gypsum pseudomorphs, stable isotopic values (n=8) in Ca-2 calcite are $\delta^{13}C$ = -7.74/-4.88‰ VPDB (reaching -10.88‰ VPDB in MAG) and $\delta^{18}O$ =-9.73/-6.14‰ VPDB, with extreme values of $\delta^{13}C$ = -3.02‰ VPDB in MAG and $\delta^{18}O$ = -15.76‰ VPDB in a slightly Fe-rich sample of CSP (Table 1, Figs. 6, 7).

$^{87}Sr/^{86}Sr$ values are very homogeneous in both calcite and dolomite micritic matrix with a mean value of 0.7082 (n=6, MAG, CSP) (Table 2).

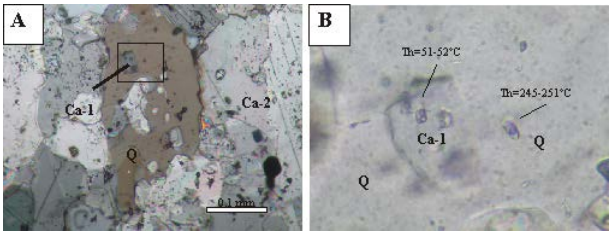

Figure 8. Photomicrographs of Ca-1 and quartz in gypsum pseudomorph. In the box appears the area magnified in **B**. Notice the corrosion of quartz by Ca-2 **(A)** and the lower T_h of the fluid inclusion in the inclusion of Ca-1 compared to fluid inclusion in quartz.

4.3. Fluid inclusion data

Fluid inclusions in the minerals that form the gypsum pseudomorphs were characterized petrographically and followed by microthermometric analysis. In order to characterize the fluid composition and temperature history, Ca-1 calcite (early) quartz (later) and Ca-2 calcite (latest) were selected for analysis of fluid inclusions.

Fluid inclusions are very scarce in the small crystals of Ca-1 (40-100 μm). For this reason, only one fluid inclusion could be studied in Ca-1. This inclusion has a large size relative to the size of the crystal and appears isolated (Fig. 8); thus, it is most reasonably characterized as primary. It yields T_h of 51-52°C.

The quartz contains fluid inclusion assemblages (FIAs) of biphasic inclusions with sizes ranging between 2-14 μm (Fig. 9**A**, Table 3). These FIAs show no relationship to growth patterns, and some are distributed along planar arrays, or appear in different planes, indicating a probable secondary origin (Fig. 9**A**). In FIAs, inclusions have variable liquid: vapor ratios: 15 to 40 vol% vapor and no vapor-dominant inclusions were found (Table 3). In addition, petrographically paired vapor-rich and vapor-poor inclusions were not observed. Homogenization temperatures are variable within each FIA, and range from 147-351°C (n=27, Fig. 10), with higher T_h in the deeper samples (Table 3). Due to the small size of the fluid inclusions, very few final melting of ice measurements (Tm_{ice}) have been recorded (n=7). They vary between -5.8 and -1.6°C among different samples. Final melting temperatures of clathrate are typically between 5 and 10°C (Ta-

Table 1. Stable isotope data of carbonate matrix and Ca-2 in gypsum pseudomorphs.

Sample	$\delta^{13}C$ (‰VPDB)	$\delta^{18}O$ (‰VPDB)		Formation
PRA-03	-6.01	-8.09	Ferroan dolomitic matrix	Fluvial
ARZA-05	-4.67	-7.77	Calcite matrix	Carbonate lake
ARZA-05	-4.52	-7.44	Calcite matrix	Carbonate lake
MAG-02	-5.53	-9.54	Dolomitic matrix	Fluvial
MAG-06	-7.47	-9.43	Calcite matrix	Carbonate lake
MAG-06	-6.95	-9.35	Calcite matrix	Carbonate lake
MAG-06	-7.56	-9.90	Calcite matrix	Carbonate lake
MAG-07	-4.14	-9.36	Calcite matrix	Alkaline lake
MAG-07	-4.51	-9.26	Calcite matrix	Alkaline lake
MAG-11	-6.11	-1.48	Dolomitic matrix	Alkaline lake
MAG-12	-6.67	-7.30	Calcite matrix	Alkaline lake
MAG-14	-6.59	-0.94	Dolomitic matrix	Alkaline lake
MAG-14	-6.54	-1.39	Dolomitic matrix	Alkaline lake
MAG-14	-10.88	-3.02	Pseudomorph	Alkaline lake
SAN-18	-6.46	-8.90	Calcite matrix	Carbonate lake
SAN-19	-6.32	-9.04	Calcite matrix	Carbonate lake
SAN-19	-6.04	-8.28	Pseudomorph	Carbonate lake
SAN-20	-6.87	-8.64	Calcite matrix	Carbonate lake
SAN-25	-7.38	-11.19	Ferroan dolomitic matrix	Carbonate lake
SAN-26	-6.93	-7.76	Dolomitic matrix	Carbonate lake
SAM-33	-4.14	-7.25	Dolomitic matrix	Alkaline lake
SAN-33	-4.88	-8.05	Pseudomorph	Alkaline lake
SAN-35	-6.87	-7.62	Pseudomorph	Alkaline lake
SAN-36	-6.11	-7.84	Pseudomorph	Alkaline lake
SAN-36	-4.73	-7.64	Dolomitic matrix	Alkaline lake
CSP-101	-4.68	-4.87	Dolomitic matrix	Alkaline lake
CSP-101	-5.52	-15.76	Pseudomorph	Alkaline lake
CSP-101	-7.69	-9.73	Pseudomorph	Alkaline lake
CSP-103	-7.74	-6.14	Pseudomorph	Alkaline lake
CSP-103	-5.60	-6.08	Dolomitic matrix	Alkaline lake

Table 2. $^{87}Sr/^{86}Sr$ data of carbonate matrix in pseudomorphs bearing samples.

Sample	$^{87}Sr/^{86}Sr$	Matrix
MAG-12	0,708286	Calcitic
MAG-11	0,708123	Dolomitic
MAG-11-2	0,708095	Dolomitic
MAG-12-2	0,708287	Calcitic
CSP-101	0,708233	Dolomitic
CSP-103	0,708208	Dolomitic

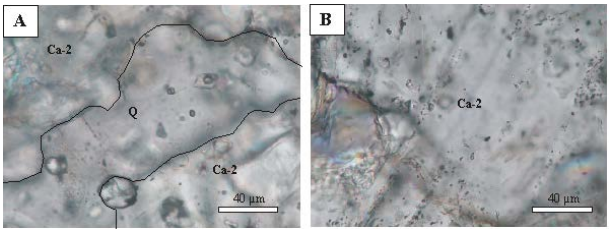

Figure 9. Photomicrographs of fluid inclusions in quartz and Ca-2. **A.** Secondary biphasic fluid inclusions in quartz distributed in different planes. The line separates quartz and Ca-2 in order to facilitate their distinction. **B.** Secondary fluid inclusions in Ca-2 distributed along planar arrays.

ble 3). Nucleation of clathrate was detected from -53 to -58°C in some fluid inclusions.

Ca-2 contains FIAs which appear in different planes that are unrelated to growth patterns. Thus, we consider them of secondary origin. They have very irregular shapes and variable sizes (1-16 µm). In addition to FIAs with all-liquid fluid inclusions, there are also FIAs with biphasic fluid inclusions of small size (typically 2-6 µm) and

Table 3. Microthermometry data of secondary fluid inclusions in quartz. Samples SAN-33, SAN-35 and CSP-101. Units: size: μm; T_h, T_n, T_n(cl), T_m(ice), T_m(cl): °C; Salinity[1]: following [32] and Salinity[2]: following [33], both measured in NaCl wt % eq.
* Fluid inclusions with enough data for calculating the salinity using clathrate equation of state.

Sample	FI	FIA	Size	L:V	Th	Tn	Tmice	Salinity[1]	Salinity[2]	Tn cl	Tm cl
SAN-35	1	1	6	70:30	178.0-182.0	-44	-2.9/-3.0	4.80-4.96	-	-	-
	2	2	4	70:30	147.0-149.0	-	-	-	-	-	-
	3	2	8	80:20	155.0-157.0	-	-	-	-	-	-
	4	2	3	80:20	165.0-173.2	-	-	-	-	-	-
	5	3	2	70:30	220.0-223.0	-	-	-	-	-	9.4
	6	4	13	80:20	208.0-209.5	-	-	-	-	-	-
	7	5	7	70:30	295.0-297.5	-	-	-	-	-	-
	8	6	8	40:60	>350	-	-	-	-	-30	5.8-8.7
	9	6	4	50:50	>350	-	-	-	-	-31	6.8-10.1
	10	6	2	70:30	254.0-260.0	-	-	-	-	-	-
	11	7	3	70:30	-	-	-1.6/-1.9	2.74-3.23	-	-	-
*	12	8	11	80:20	-	-38	-4.7/-4.9	7.45-7.73	4.9	-30	2.9-6.6
SAN-33	1	1	6	80:20	252.8-260.8	-	-	-	-	-29	-
	2	1	5	80:20	260.4-266.4	-	-	-	-	-29	8.6
	3	1	3	70:30	277.0-285.2	-	-	-	-	-29	8.8
	4	2	3	60:40	322.0-329.0	-	-	-	-	-	-
	5	3	-	70:30	280.0-286.7	-	-	-	-	-	-
	6	4	12	80:20	210.0-220.4	-	-	-	-	-	-
	7	5	3	85:15	299.0-301.6	-	-	-	-	-43	-
	8	5	4	80:20	340.4-351.0	-	-	-	-	-29	9.5
	9	6	6	80:20	235.0-240.0	-30	-	-	-	-51	8.6
CSP-103	1	1	3	80:20	136.0-146.0	-	-	-	-	-	-
	2	2	4	80:20	341.6-351.5	-33	-4.9/-4.7	7.45-7.73	-	-58	-5.4/-4.9
*	3	2	5	80:20	294.0-297.0	-	-4.7?	7.45	5.1	-53	0.3-5.0
	4	2	4	75:25	166.0-172.0	-	-2.5?/-3.0?	4.18-4.96	-	-54	-9.7/-13.6
	5	3	8	80:20	245.0-251.0	-	-	-	-	-	-
	6	3	8	75:25	165.0-170.0	-41	-5.6/-5.8	8.68-8.95	-	-	-

variable liquid:vapor ratio: 10 to 40 vol% vapor (Fig. 9**B**, Table 4). Again, petrographic pairing or vapor-dominant inclusions were not found. T_h measured in these FIAs range from 108 to 352°C (n=25, Fig. 10**A** and **B**) with T_m(ice) of -0.1°C (n=5) (Table 4).

As can be shown in the histograms, there is high variability of T_h data among the same FIAs in all samples, for both fluid inclusions in quartz and Ca-2 (Fig. 10).

5. Discussion

On the basis of the paragenetic, fluid inclusion, and geochemical data we have established different stages in the fluid and thermal history that include: (1) deposition in lake; (2) early burial; (3) late burial; (4) hydrothermalism; and (5) unroofing and cooling (Figure 11).

5.1. Syndepositional through intermediate burial diagenesis

Lenticular gypsum is considered to form early and syndepositionally with evaporative conditions or either marine or nonmarine origin. Although the succession has been shown to be dominantly lacustrine, there is evidence for a possible marine incursion towards the SW of the study area [15]. The $^{87}Sr/^{86}Sr$ analyses from carbonate matrix of gypsum pseudomorphs in two stratigraphic sections from the southern end of the study area (MAG, CSP) can help to assess if matrix around the gypsum is marine or nonmarine in origin (Table 1). The $^{87}Sr/^{86}Sr$ data measured is 0.7082 (mean value, n=6) whereas Tithonian-Berriasian marine data of Veizer et al. (1999) [35] range from 0.7065 to 0.7075. This lends support for a nonmarine origin for the matrix, although we cannot rule out diagenetic resetting. In addition, we have not observed any sedimentary evidence for the marine influence in this area. Thus, we

Table 4. Microthermometry data of secondary fluid inclusions in calcite. Samples SAN-33 and SAN-35. Units: size: μm; T_h, T_n, T_m(ice), T_m(cl):°C; Salinity: NaCl wt % eq. following [32]

Sample	FI	FIA	Size	L:V	Th	Tn	Tmice	Salinity	Tn cl
SAN-35	1	1	–	85:15	174.5-176.5	–	–	–	–
	2	1	–	80:20	150.0-156.0	–	–	–	–
	3	1	–	–	155.0-160.0	–	–	–	–
	4	1	–	70:30	225.0-229.0	–	–	–	–
	5	2	–	80:20	217.0-218.5	–	–	–	–
	6	3	7	80:20	193.0-195.0	–	–	–	–
	7	3	9	70:30	285.0-288.0	–	–	–	–
	8	3	10	80:20	231.0-237.0	–	–	–	–
	9	4	–	80:20	240.0-243.0	-39	-0.1	0.18	–
	10	5	–	80:20	229.0-231.0	–	–	–	–
	11	6	6	85:15	211.0-214.0	-39	-0.1	0.18	–
	12	6	10	70:30	242.0-247.0	–	-0.1	0.18	–
	13	6	4	80:20	242.0-247.0	–	–	–	–
	14	6	5	80:20	233.0-236.0	-39	-0.1	0.18	–
	15	7	–	70:30	321.0-326.0	-40	-0.1	0.18	–
	16	8	4	70:30	180.0-182.7	–	–	–	–
	17	9	2	80:20	198.0-204.0	–	–	–	–
	18	9	3	80:20	190.0-194.2	–	–	–	–
	19	9	3	80:20	195.2-200.1	–	–	–	–
	20	9	4	70:30	229.3-232.8	–	–	–	–
	21	10	6	75:25	–	-46	–	–	–
SAN-33	1	1	13	90:10	108.0-116.0	–	–	–	–
	2	2	11	60:40	278.0-282.0	–	–	–	–
	3	2	9	70:30	266.0-271.0	-39?	–	–	-39?
	4	3	10	50:50	350.0-352.0	–	–	–	–

consider more plausible that lenticular gypsum and its surrounding matrix formed in shallow alkaline ephemeral lakes.

On the basis of the fossil content and associated facies presented, a lacustrine depositional environment is widely accepted for most of the section. No significant differences are observed when comparing the stable isotope data among carbonate facies or among different stratigraphic sections (Figs. 6, 7), with the exception of three dolomite samples at the top of MAG section (Fig. 1), with $\delta^{18}O$ around -1 VPDB‰. These samples are from the uppermost deposits of shallow alkaline ephemeral lakes, and they are clearly enriched in $\delta^{18}O$ if compared to the rest of the alkaline lake samples (Figs. 6, 7). As the marine influence is unlikely on the basis of Sr isotope data, we interpret these less negative values of $\delta^{18}O$ to be a product of strong evaporation. As early gypsum precipitation reduces sulphate and increases Mg/Ca in solution, dolomitization could be favoured, eg: [36]. The occurrence of the inferred early dolomitization at the end of alkaline lacustrine sedimentation can be an indicator of an evaporation increase probably related to a climatic change during the Berriasian in the studied area.

Anhydrite solid inclusions in quartz and Ca-2 are pointing to gypsum anhydritization. This process probably occurred during shallow burial (Fig. 3), because if gypsum had preserved until significant burial depths, them there should have been some plastic deformation and modification of crystal forms. Although primary surface and near-surface anhydrite has been described [37, 38] we can rule out this hypothesis because of lenticular shape is characteristic of gypsum crystals. The gypsum must have subsequently been transformed to anhydrite before further replacement, and this dehydration is to be expected during shallow burial and increasing temperature.

The other very early replacement is Ca-1. It has a non-ferroan composition consistent with oxidized waters [39]. Its position in the diagenetic sequence is before quartz and the only primary aqueous inclusion measureable had low T_h (51-52°C). Both facts are pointing to the early replacement of anhydrite (Fig. 11). One could posit that preservation of such a low-temperature fluid inclusion, in a weak mineral such as calcite, might be surprising con-

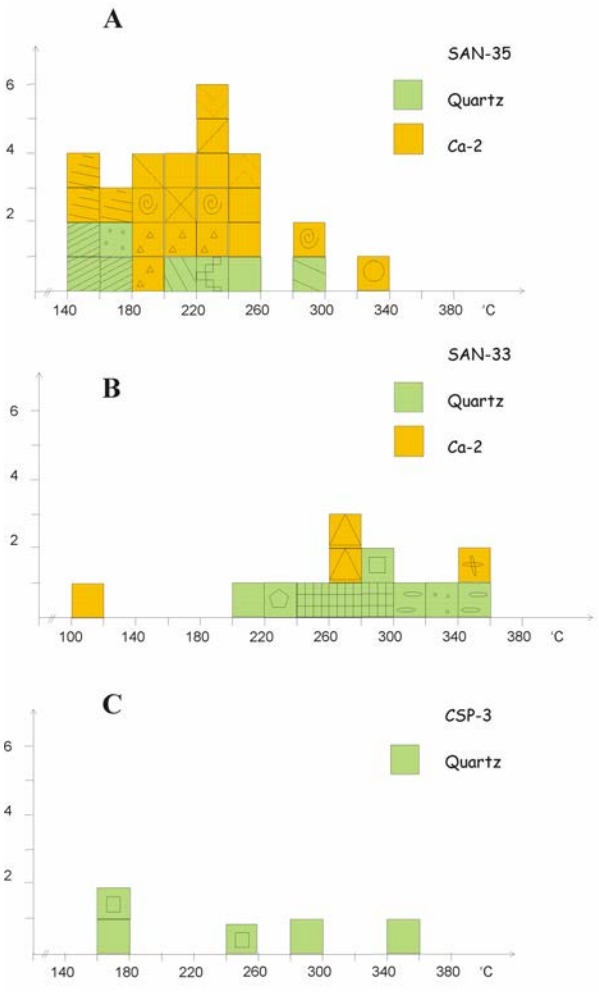

Figure 10. Histograms of T_h of fluid inclusions in quartz and Ca-2. Each FIA marked with a different pattern. Vertical axis indicates number of fluid inclusions.

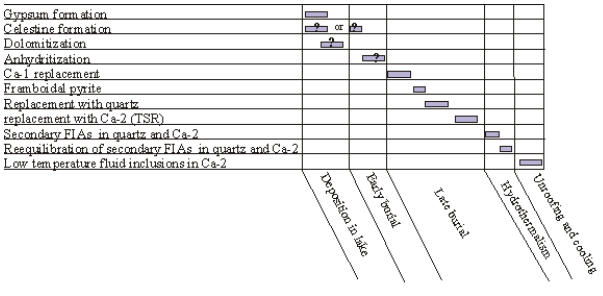

Figure 11. Relative chronology of the different synsedimentary, diagenetic and hydrothermal processes and products. Deposition in lake corresponds to Tithonian- Berriasian and hydrothermalism with Late Albian to Coniacian.

sidering its entrapment during prograde conditions. Its preservation, however, might be the result of the fluid inclusion's occurrence within a small calcite crystal surrounded by a single, stronger, crystal of quartz.

The origin of celestine is more complex, because primary bioinduced precipitation of celestine in evaporitic environments has been described [40–42], as well as a by-product of anhydrite hydration [43–46]. Furthermore, hydrothermal celestine has been documented [47]. The anhydrite hydration hypothesis is unlikely because there is no petrographic evidence of this and because anhydrite relicts are protected inside quartz and Ca-2. The hydrothermal origin is also unlikely in our case, on the basis of crystal morphology and paragenetic position. Thus, we consider it is more probable that celestine is a primary precipitate or at least has a very early diagenetic origin as a replacement of gypsum. Celestine may have been preserved because its solubility is lower than that of gypsum [48]. As no relationship has been observed between anhydrite, celestine and Ca-1 solid inclusions we are unable to establish the chronology among them. Finally, pyrite crystals probably predate both quartz and Ca-2 (Fig. 11), because are commonly observed in the inner boundaries of the pseudomorphs.

The observations indicate early gypsum precipitation associated with an evaporitic lake environment, and possibly associated with early dolomitization (Fig. 11). This was followed by replacement with Ca-1, and anhydrite in a shallow burial environment, likely no more than tens of degrees C higher than depositional temperatures.

5.2. Diagenesis during late burial and hydrothermal metamorphism

In gypsum pseudomorphs replacement proceeded with quartz followed by Ca-2 calcite. Other studies in the area demonstrate syntaxial quartz precipitation during progressive deep burial and in fracture fills associated with later hydrothermal processes [26]. First quartz formation in this area (SAN, Fig. 1) proceeded at high temperatures after depths of approximately 3 km were reached, after the late Barremian. This timing consideration is based on previous work of the authors [26], considering petrography and fluid inclusion microthermometry in quartz in relation to burial history and geothermal gradients. On this basis, quartz replacement in pseudomorphs is hypothesized to be coeval with syntaxial quartz overgrowths in sandstones or fracture fills, associated with deep burial and the first stages of Cretaceous hydrothermalism.

Later, Ca-2 calcite replacement likely also proceeded at higher temperature. Ca-2 stable isotopic data can be used to further constrain the conditions of Ca-2 precipitation.

The light $\delta^{13}C$ (-5.0 to -11.0‰) values in Ca-2 (figs 6, 7) are supportive of breakdown of organic matter due to thermochemical reduction of sulphate [49, 50] or bacterial sulphate reduction [3]. The presence of pyrite and the fetid smell when breaking samples is consistent with sulphate reduction. Typical temperatures expected for thermochemical sulphate reduction are greater than 100°C [50], and it is expected that Ca-2 formed at or above this temperature. The petrographic observations do not support a shallow depth for Ca-2, and thus, the low-temperature bacterial sulphate reduction hypothesis is unlikely. In addition, the most negative values of $\delta^{18}O$ in Ca-2 (-15.76‰ VPDB) also indicate high temperatures. Both Ca-2 and matrix data are highly scattered and suggest some degree of isotopic reset at high temperature. Thus, replacement of quartz with Ca-2 probably took place well after quartz began precipitating; i.e. after burial deeper than 3 km.

Secondary fluid inclusions in quartz and Ca-2 provide a record of the temperatures and salinities of post-precipitation fluids. No FIAs with consistent T_h have been observed. Neither petrographically paired vapor-rich and vapor-poor inclusions nor vapor-dominant inclusions were observed in quartz and Ca-2 cements, so there is no evidence for necking down after a phase change nor evidence of heterogeneous entrapment (e.g. [30]).

The high *T*h values and the inconsistency within FIAs (Fig. 5) measured in secondary fluid inclusions in quartz (147-351°C) and calcite (108-352°C) demonstrate that both minerals experienced high temperatures after their formation and after entrapment of originally lower temperature FIAs. The temperatures are in the same range as other thermally reequilibrated fluid inclusions measured in thick quartz veins in the same area, related to a Cretaceous hydrothermal processes that affected this part of basin [26]. As the quartz precipitation postdates deep burial in the area, and some formed during hydrothermal thermal metamorphism, we consider that the secondary fluid inclusions were formed after deep burial and perhaps during hydrothermal thermal metamorphism. Clearly, thermal reequilibration of these inclusions indicates their alteration during one or more pulses of hydrothermal metamorphism that postdated entrapment of the secondary fluid inclusions at a lower, yet still quite high, temperature.

The salinities of the high-temperature fluid inclusions in quartz, would be interpreted to be between 2.74 to 7.73 NaCl wt % eq. (Table 3), without consideration of clathrates [32]. As first melting temperatures are close to the metastable eutectic for the NaCl-H_2O (observed around -29/-31°C), the NaCl-H_2O model system is in part appropriate. Other studies in the region, however, demonstrated that fluids associated with the hydrothermal quartz [26], were rich in CO_2. Our data of show clathrate nucleation events between -53 and -58°C and formation of significant amounts of clathrate (Table 3) in high temperature fluid inclusions offers support for significant amounts of CO_2. The presence of clathrates would indicate that bulk salinities would be lower than those calculated from T_m(ice) measurements using the NaCl-H_2O model system. In inclusions in which the appropriate microthermometric measurements can be made, use of the NaCl-H_2O-CO_2 model system indicates salinities around 5 wt % NaCl. The calculations employed the ICE software [33] (Table 3). The Tm_{ice} measurements in Ca-2 FIAs with high T_h values are commonly close to 0°C (Table 4), indicating salinities significantly lower than those in quartz FIAs. Paragenetic position and stable isotopic composition of Ca-2, and high T_h values in these inclusions support formation and reequilibration of fluid inclusions after deep burial. Fluid inclusion salinities that vary from those in quartz support the idea of variable salinities during pulses of hydrothermal fluid flow.

5.3. Uplift and cooling

The thermal and fluid record concludes with uplift and unroofing manifested by the presence of secondary all-liquid FIAs in Ca-2.

6. Conclusions

1. A complex geological history can be ascertained from replacements of gypsum crystals that originally formed in an alkaline lake system. It is the chemical malleability of the gypsum and subsequent minerals and fluid inclusions that are advantageous in recording multiple events in the geologic history through partial resetting during recrystallization or thermal reequilibration.

2. The history starts with deposition in a nonmarine lacustrine system that evolves to an evaporative system through time. This results in dolomitization and lenticular gypsum precipitation syndepositionally with the lake. Shallow to intermediate burial includes anhydritization of primary gypsum, celestine precipitation, and non-ferroan calcitization, all at relatively low temperatures.

3. During deep burial and hydrothermalism, pseudomorphs are partially replaced by quartz and then calcite Ca-2. On the basis of regional evidence quartz precipitates at high temperature after Late Berriasian, deeper than 3 km, from a highly saline

fluid. It is followed by calcitization associated with thermochemical sulphate reduction at high temperature, on the basis of isotopic data.

4. The main replacement phases (quartz and Ca-2) contain secondary fluid inclusions reequilibrated during later hydrothermal processes (T_h = 108-352°C) with intermediate and low salinities. In case of quartz there was presence of dissolved CO_2.

5. Fracturing and fluid inclusion entrapment continues during uplift at low temperature.

6. This extensive record of fluid and thermal history is gleaned from materials that are partially replaced and partially reequilibrated. It is partial alteration that works in favour of developing this record. Partial alteration and thermal reequilibration may prove to be our friends rather than enemies in such studies.

Acknowledgements

Funding for this research was provided by the Spanish DIGICYT projects BTE 2001-026, CGL 2005-07445-C03-02/BTE and CGL2008-01648/BTE, and by UCM-CM (Universidad Complutense-Madrid Community) for the Research Group "Sedimentary Basin Analysis". The authors would like to thank M.E. Sanz-Montero and P. Lecumberri for their useful suggestions and M.A. Barajas for technical support.

References

[1] Cody R.D., Lenticular gypsum: occurrences in nature, and experimental determinations of effects of soluble green plant material on its formation. *J. Sediment. Petrol.*, 1979, 49, 1015-1028

[2] Ulmer-Scholle D.S., Scholle P.A., Replacement of evaporites within Permian Park City Formation. Bighorn Basin. Wyomig, USA. *Sedimentology*, 1994, 41, 1203-1222

[3] Anadón P., Rosell L., Talbot M.R., Carbonate replacement of lacustrine gypsum deposits in two Neogene continental basins, eastern Spain. *Sediment. Geol.*, 1992, 78, 201-216

[4] Mas J.R., Alonso A., Guimerá J., Tectosedimentary evolution of an extensional intraplate basin: the Late Jurassic-Early Cretaceous Cameros Basin (La Rioja-Soria). Evolución tectonosedimentaria de una cuenca extensional intraplaca: la Cuenca de Los Cameros (La Rioja- Soria). *Rev. Soc. Geol. Esp.*, 1993, 6, 129-144 [in Spanish].

[5] Guimerá J., Alonso A., Mas J.R., Inversion of an extensional-ramp basin by a newly formed thrust: the Cameros Basin (N Spain). In: Buchanan, J.G., Buchanan, P.G. (Eds.), Basin Inversion. *Geol. Soc. Spec. Publ.*, 1995, 88, 433-453

[6] Salas R., Guimerá J., Mas J.R., Martín-Closas C., Meléndez A., Alonso A., Evolution of the Mesozoic Central Iberian Rift System and its Cainozoic Inversion (Iberian Chain). In: Cavazza W., Roberson A.H.F.R., Ziegler P. (Eds.), Peri-Tethyan Rift- Wrench Basins and Passive Margins. Mémoires du Muséum National d'Histoire Naturelle, Paris, 2001, 145-185

[7] Mas J.R., Benito M.I., Arribas J., Serrano A., Guimerà J., Alonso A., Alonso-Azcárate J., La Cuenca de Cameros: desde la extensión finijurásica-eocretácica a la inversión terciaria – Implicaciones en la exploración de hidrocarburos. The Cameros Basin: from the Late Jurassic – Early Cretaceous extension to the Tertiary inversion – implications in hydrocarbon exploration. *Zubía. Instituto de Estudios Riojanos*, 2002, 14, 9-64 [in Spanish]

[8] Guimerá J., Mas J.R., Alonso A., Intraplate deformation in the NW Iberian Chain: Mesozoic extension and Tertiary contractional inversion. *J. Geol. Soc. Lon.*, 2004, 161, 291-303

[9] Mas J.R., Benito M.I., Arribas J., Serrano A., Guimerá J., Alonso A., Alonso-Azcàrate J., The Cameros Basin: From late Jurassic- early Cretaceous Extension to Tertiary Contractional Inversion- Implications of Hydrocarbon Exploration. In: AAPG International Conference and Exhibition, Geological Field Trip, Barcelona, Spain, 2003

[10] Guiraud M., Seguret M., A realising solitary overstep model for the late Jurassic- Early Cretaceous (Wealdian) Soria strike-slip basin (Northern Spain). SEMP Special Publication 37, Oklahoma, 1985, 159-175

[11] Casas-Saínz A.M., Gil-Imaz A., Extensional subsidence, contractional folding and thrust inversion of the Eastern Cameros Basin, Northern Spain. *Geol. Rudsch.*, 1998, 86, 802-818

[12] Mata M.P., Casas A.M., Canals A., Gil A., Pocovi A., Thermal history during Mesozoic extension and Tertiary uplift in the Cameros Basin, northern Spain. *Basin Res.*, 2001, 13, 91-111

[13] Villalaín J.J., Fernández-González G., Casas A.M., Gil-Imaz A., Evidence of a Cretaceous remagnetization in the Cameros Basin (North Spain): implications for basin geometry. *Tectonophysic.*, 2003, 377, 101-117

[14] Casas-Saínz A.M., Villalaín J.J., Soto R., Gil-Imaz A.,

Del Río P., Fernández G., Multidisciplinary approach to an extensional syncline model for the Mesozoic Cameros Basin (N Spain). *Tectonophysics*, 2009, 470, 3-20

[15] Gómez-Fernández J.C., Meléndez N., Stratigraphy of the Cameros Basin (NW Iberian Range, N Spain) during the Jurassic-Cretaceous transit. Estratigrafía de la Cuenca de Cameros (Cordillera Ibérica noroccidental, N de España) durante el tránsito Jurásico-Cretácico. *Rev. Soc. Geol. Esp.*, 1994, 7, 121-139 [in Spanish]

[16] Martín-Closas M., Alonso-Millán A., Stratigraphy and biostratigraphy (Charophyta) of Lower Cretaceous in the western sector of the Cameros Basin (Iberian Range). Estratigrafía y Bioestratigrafía (Charophyta) del Cretácico inferior en el sector occidental de la Cuenca de Cameros (Cordillera Ibérica). *Rev. Soc. Geol. Esp.*, 1998, 11, 253-269 [in Spanish]

[17] González-Acebrón L., Arribas J., Mas J.R., Provenance of fluvial sandstones at the start of late Jurassic-early Cretaceous rifting in the Cameros Basin (N. Spain). *Sediment. Geol.*, 2007, 202, 138-157

[18] González-Acebrón L., The Tera Group in the Eastern sector of the Cameros Basin: sedimentary environments, provenance and diagenetic evolution. PhD Thesis, Universidad Complutense de Madrid, Madrid, 2009, [in Spanish]

[19] Casquet C., Galindo C., González-Casado J.M., Alonso A., Mas J.R., Rodas M., García E., Barrenechea J.F., The metamorphism in the Cameros Basin. Geochronology and tectonic implications. El metamorfismo en la cuenca de Cameros: geocronología e implicaciones tectónicas. *Geogaceta*, 1992, 11, 22-25 [in Spanish]

[20] Barrenechea F.J., Rodas M., Mas J.R., Clay mineral variation associated to diagenesis and low-grade metamorphism of early Cretaceous sediments in the Cameros Basin, Spain. *Clay Miner.*, 1995, 30, 89-103

[21] Alonso-Azcárate J., Barrenechea F.J., Rodas M., Mas J.R., Comparative study of the transition between very low-grade metamorphism and low-grade metamorphism in siliciclastic and carbonate sediments. Early Cretaceous, Cameros Basin (North Spain). *Clay Miner.*, 1995, 30, 407-419

[22] Alonso-Azcárate J., Rodas M., Bottrell S.H., Raiswell R., Velasco F., Mas J.R., Pathways and distances of fluid flow during low-grade metamorphism: evidence from pyrite deposits of the Cameros Basin, Spain. *J. Metamor. Geol.*, 1999, 17, 339-348

[23] Alonso-Azcárate J., Rodas M., Bottrell S.H., Mas J.R., Pyrite ores in the Cameros Basin. Los yacimientos de pirita de la Cuenca de Cameros, Zubía. *Instituto de Estudios Riojanos*, 2002 14, 173-190 [in Spanish]

[24] Mantilla-Figueroa L.C., Casquet C., Mas J.R., The Oncala Group paleofluids, Cameros Basin (La Rioja, Spain): fluid inclusion, oxygen isotopes and SEM data. Los paleofluidos del Grupo Oncala, Cuenca de Cameros (La Rioja, España): Datos de inclusiones fluidas, isótopos de oxígeno y SEM. *Geogaceta*, 1998, 24, 207-210 [in Spanish]

[25] Mantilla-Figueroa L.C., Casquet C., Galindo C., Mas J.R., The Cretaceous and Paleogene hydrothermal metamorphism in the Cameros Basin (Iberian Range, Spain). El metamorfismo hidrotermal Cretácico y Paleógeno de la Cuenca de Cameros (Cordillera Ibérica, España). *Zubía. Instituto de Estudios Riojanos*, 2002, 14, 143-154 [in Spanish]

[26] González-Acebrón, L., Goldstein, R.H, Arribas, J., Mas, R., Criteria for recognition of localization and timing of multiple events of hydrothermal alteration in sandstones illustrated by petrographic, fluid inclusion, and isotopic analysis of the Tera Group, Northern Spain. *Int. J.Earth Sci.*, 2011, 100, 1811-1826

[27] Barrenechea F.J., Rodas M., Frey M., Alonso-Azcárate J., Mas J.R., Chlorite, Corrensite and Chlorite- Mica in Late Jurassic Fluvio- Lacustrine sediments of the Cameros Basin of Northeastern Spain. *Clay Clay Miner.*, 2000, 48, 256-265

[28] Barrenechea F.J., Rodas M., Frey M., Alonso-Azcárate J., Mas J.R., Clay diagenesis and low-grade metamorphism of Tithonian and Berriasian sediments in the Cameros Basin. *Clay Miner.*, 2001, 36, 325-333

[29] Del Río, P., Barbero, L., Mata, P., Fanning, C.M. Timing of diagenesis and very low-grade metamorphism in the eastern sector of the Sierra de Cameros (Iberian Range, Spain): a U-Pb SHRIMP study on monazite. *Terra Nova*, 21, 438-445

[30] Goldstein R.H., Reynolds T.J., Systematics of fluid inclusions in diagenetic minerals. SEMP Short Course, 31, Oklahoma City, 1994

[31] Goldstein R.H., Fluid Inclusion Geothermometry in Sedimentary Systems: From Paleoclimate to Hydrothermal. In: Harris N. (Ed.), SEPM Special Publication, Thermal History Analysis of Sedimentary Basins, Oklahoma City, (in press)

[32] Bodnar R.J., Revised equation and Table for determining the freezing point depression of H_2O-NaCl solutions. *Geochim. Cosmochim. Ac.*, 1993, 57, 683-684

[33] Bakker R.J. Clathrates: computer program to calculate fluid inclusion V-X using clathrates melting temperatures. *Computer and geosciences,* 1997, 26, 1-17

[34] Lindholm R.C., Finkelman R.B., Calcite staining:

semiquantitative determination of ferrous iron. *J. Sediment. Petrol.*, 1972, 42, 239-245

[35] Veizer J., Ala D., Azmy K., Bruckschen P., Buhl D., Bruhn F., Carden G.A.F., Diener A., Ebneth S., Godderis Y., Jasper T., Korte K., Pawellek F., Podlaha O.G., Strauss H., Sr^{87}/Sr^{86}, δC^{13} and δO^{18} evolution of Phanerozoic seawater. *Chem. Geol.*, 1999, 161, 59-88

[36] McKenzie J., Holocene dolomitization of calcium carbonate sediments from the coastal sabkhas of Abu Dhabi, U.A.E.: A stable isotope study. *J. Geol.*, 1981, 89, 185-198

[37] Ortí F., Rosell L., Crystalline fabrics of nodular and laminated anhydrite. Fábricas cristalinas de la anhidrita nodular y laminada. *Acta Geologica Hispánica*, 1981, 16, 235-255 [in Spanish]

[38] Schreiber B.C., El Tabakh M., Deposition and early alteration of evaporites. *Sedimentology*, 2000, 47 (Suppl. 1), 215-238

[39] Meyers W.J., Carbonate cement stratigraphy of the Lake Valley Formation (Missisipian) Sacramento Mountains, New Mexico. *J. Sediment. Petrol.*, 1974, 44, 837-861

[40] Schultze-Lam S., Douglas T., Thomson J.B., Beveridge T.J., Metal ion immobilization by bacterial surfaces in freshwater environment. *Water Pollut. Res. J. Canada*, 1993, 28, 51-81

[41] Douglas S., (2002): ESEM-EDS and XRD study of micromineralogical layering in a microbial mat from a hypersaline pond on Lee Stocking Island, Bahamas: formation of celestine in microbial exopolymers. Paper presented at Annual meeting of the Geological Society of America, Denver, USA, 27-30, 2002

[42] Sanz-Montero M.E., Rodríguez-Aranda J.P., García del Cura M.A., Bioinduced precipitation of barite and celestine in dolomite microbialites. Examples from Miocene lacustrine sequences in the Madrid and Duero Basins, Spain. *Sediment. Geol.*, 2009, 222, 138-148

[43] Dean W.E., Trace of minor elements in evaporites. In: Dean W.E., Schreiber B.C., (Eds.), Marine Evaporites. SEPM Short Course 4. Society of Economic Palaeontologists and Mineralogists, Oklahoma City, 1978, 86–104

[44] Kasprzyk A., Sedimentological and diagenetic patterns of anhydrite deposits in the Badenian evaporite basin of the Carpathian Foredeep, southern Poland. *Sediment. Geol.*, 2003, 158, 167–194

[45] Gündogan I., Önal M., Depçi T., Sedimentology, petrography and diagenesis of Eocene–Oligocene evaporites: the Tuzhisar Formation, SW Sivas Basin, Turkey. *J. Asian Earth Sci.*, 2005, 25, 791–803

[46] Dill H.G., Henjes-Kunst F., Berner Z., Stüben D., Miocene diagenetic and epigenetic strontium mineralization in calcareous series from Cyprus and the Arabian Gulf: Metallogenic perspective on sub- and suprasalt redox-controlled base metal deposits. *J. Asian Earth Sci.*, 2009, 34, 557–576

[47] Tekin E., Varol B., Ayan Z., Satir M., Epigenetic origino f celestine deposits in the Tertiary Sivas Basin: new mineralogical and geochemical evidence. *N. Jb. Miner. Mh.*, 2002, 7, 289-318

[48] Warren J.K., Evaporites: Sediments, Resources and Hydrocarbons. Springer, Berlin, 2006

[49] Kendal A.C., Late diagenetic calcitization of anhydrite from Mississippian of Saskatchewan, western Canada. *Sedimentology*, 2001, 48, 29-55

[50] Machel H.G., Krouse R.H., Sassen R., Products and distinguishing criteria of bacterial and thermochemical sulphate reduction. *Appl. Geochem.*, 1995, 10, 373-389